Biophysical *Journal*
Article

Biophysical Society

Influence of microflow on hepatic sinusoid blood flow and red blood cell deformation

Tianhao Wang,[1] Shouqin Lü,[2,3] Yinjing Hao,[1] Zinan Su,[1] Mian Long,[2,3,*] and Yuhong Cui[1,*]
[1]School of Mechanical Engineering, Tianjin University, Tianjin, China; [2]Center of Biomechanics and Bioengineering, Key Laboratory of Microgravity (National Microgravity Laboratory), Beijing Key Laboratory of Engineered Construction and Mechanobiology, Institute of Mechanics, Chinese Academy of Sciences, Beijing, China; and [3]School of Engineering Science, University of Chinese Academy of Sciences, Beijing, China

ABSTRACT Hepatic sinusoids present complex anatomical structures such as the endothelial sieve pores and the Disse space, which govern the microscopic blood flow in the sinusoids and are associated with structural variations in liver fibrosis and cirrhosis. However, the contributions of the permeability of endothelial and collagen layers and the roughness of hepatocyte microvilli to the features of this microflow remain largely unknown. Here, an immersed boundary method coupled with a lattice Boltzmann method was adopted in an in vitro hepatic sinusoidal model, and flow field and erythrocyte deformation analyses were conducted by introducing three new source terms including permeability of the endothelial layer, resistance of hepatocyte microvilli and collagen layers, and deformation of red blood cells (RBCs). Numerical calculations indicated that alterations in endothelial permeability could significantly affect the flow velocity and flow rate distributions in hepatic sinusoids. Interestingly, a biphasic regulating pattern of shear stress occurred simultaneously on the surface of hepatocytes and the lower side of endothelium, i.e., the shear stress increased with increased thickness of hepatocyte microvilli and collagen layer when the endothelial permeability was high but decreased with the increase of the thickness at low endothelial permeability. Additionally, this specified microflow manipulates typical RBC deformation inside the sinusoid, yielding one-third of the variation of deformable index with varied endothelial permeability. These simulations not only are consistent with experimental measurements using in vitro liver sinusoidal chip but also elaborate the contributions of endothelial and collagen layer permeability and wall roughness. Thus, our results provide a basis for further characterizing this microflow and understanding its effects on cellular migration and deformation in the hepatic sinusoids.

SIGNIFICANCE As the basic unit of the liver, the blood flow in hepatic sinusoids is crucial to liver functions. Owing to the complicated anatomical structures with the featured endothelial sieve pores and Disse space underneath the endothelium, the microflow dynamics in the in vivo sinusoids and the in vitro liver chips is still challenging. We developed a hepatic sinusoidal model by applying microflow approaches and performed flow field analyses by introducing source terms including the permeability of endothelial layer, the resistance of hepatocyte microvilli and collagen layers, and the deformation of erythrocytes. The biphasic pattern of shear stress on the hepatocyte and endothelial cells surface was uncovered. These results highlight the importance of microflow effects in hepatic sinusoids and liver chips.

INTRODUCTION

Blood flow in hepatic sinusoids is highly associated with the functionality of the liver. These sinusoids serve as the basic unit of the liver, and the blood flow in sinusoids is crucial to many functions, such as protein synthesis, enzyme synthesis, and toxin metabolism (1,2). These sinusoids are composed of hepatocytes, liver sinusoidal endothelial cells, and other nonparenchymal cells such as stellate cells and Kupffer cells and have a specialized microstructure and physical microenvironment (3–5), which makes blood flow in these regions different from the general capillary blood flow (6,7). Specifically, there is a gap between the endothelial cells and hepatocytes, called the Disse space, 1 μm in diameter. Blood flows into the Disse space through the sieve pores in the

Submitted March 30, 2021, and accepted for publication September 10, 2021.

*Correspondence: mlong@imech.ac.cn or yhcui@tju.edu.cn
Tianhao Wang and Shouqin Lü contributed equally to this work.

Editor: Mark Alber.
https://doi.org/10.1016/j.bpj.2021.09.020

endothelium, implementing mass transfer and signal exchange with hepatocytes. When the characteristic size of flow is reduced to micro dimensions, the secondary fluid flow phenomena that are negligible in macroscopic flow attains primary status in microflow (8,9), and the related regulating factors such as wall roughness in sinusoids cannot be ignored. Physiologically, the existence of numerous microvilli on the surface of hepatocytes aggravates the effect of surface roughness on blood flow and modulates the distribution of blood flow shear stress in the Disse space. When liver fibrosis occurs, the endothelial cell layer appears capillarized, subcutaneous basement membrane is formed, and endothelial sieve pores disappear, altering the permeability of the endothelium and leading to changes in its percolation and in blood flow in the Disse space. Meanwhile, the presence of a large amount of collagen filling in the Disse space alters the effects of the original hepatocyte microvilli on blood flow and further abolishes mass transfer and mechanotransduction between blood flow and hepatocytes (3–5). Therefore, it is critical to elucidate the microflow features of blood flow in the sinusoid in different pathophysiological scenarios and quantify the effects of various regulating factors, such as the hepatic microvillus, sieve pores, and micro size of the Disse space in hepatic sinusoids.

To date, both experimental approaches and theoretical modeling have been applied to examine the physiological structure and blood flow characteristics of hepatic sinusoids. For example, an in vivo system was built to experimentally observe the tissue morphology of sinusoids in mice without dealing with the blood flow changes (10). Two-photon fluorescence microscopy was used to visualize blood flow in the superficial vessels in mice with fatty liver and elucidate blood flow changes in hepatic sinusoids under normal and pathological conditions (11). However, in vivo observations in humans are still difficult because of the need for laparotomy and fluorescent staining of venous vessels. Meanwhile, spatial resolution limitations and in-depth measurement difficulties prevent effective observations of in vivo blood flow in such microsized structures as hepatic sinusoids and the effects of hepatocyte microvilli and collagen deposit on blood flow. Ex vivo liver tissues obtained from surgery can be used to monitor collagen deposition and histological morphology in liver sinusoids under normal and pathological conditions using transmission electron microscopy (3); however, blood flow in hepatic sinusoids and blood flow changes before and after lesion formation could not be obtained in such scenarios. Evidently, direct experimental studies on hepatocyte microvilli and other microflow issues in hepatic sinusoids remain difficult to perform.

In recent years, multiple in vitro liver chip models have been developed to mimic in vivo anatomical structures to facilitate the understanding of the physiological functions and toxicant metabolism of hepatocytes. For example, the dual-channel structure and porous permeable membrane in a typical liver chip model can simulate the spatial configuration of hepatocytes and endothelial cells and represent the flow features across endothelial cells in sinusoids (12–14). In one of our previous studies, the effects of shear stress on fluid flow distributions were tested on the coculture of hepatocytes and endothelial cells, providing a basis for estimating blood flow in hepatic sinusoids (14). Noting that the properties of the liver chip model are still far from an in vivo hepatic sinusoid, flow features in hepatic sinusoids, especially at the micro scale, need to be investigated further. When the size of the liver chip reaches micron level, the influence of microflow becomes apparent, especially in the lower flow channel of the liver chip where the impacts of wall roughness could be prominent because of the low flow velocity. Thus far, this microflow factor has not been taken into account, and further studies are needed to investigate the characteristics of microflow in liver chips.

Because of the difficulties and limitations of the above in vivo, in vitro, and liver chip measurements for hepatic sinusoid flow, theoretical modeling with numerical simulations has become an important method to uncover hepatic sinusoid blood flow characteristics. For example, blood flow in hepatic sinusoids was simulated in previous studies considering the effect of sieve pores; however, the effects of flow in refined structures such as the Disse space was not involved (15). Furthermore, the metabolism of serum ammonia in hepatocytes was analyzed numerically based on the effect of blood flow in a microchannel that does not contain a porous permeable membrane (16). The inflammatory response to *Salmonella* was theoretically tested in hepatic sinusoids even without considering the contributions of blood flow (17). To date, studies on numerical simulations of hepatic sinusoid blood flow characteristics are quite few, especially those on the effects of hepatocyte microvilli and micro size of Disse space on microflow features.

Herein, microflow in hepatic sinusoids was analyzed numerically, and the effects of the endothelial layer sieve pores and Disse space were elucidated in varied pathophysiological scenarios. Specific regulating factors such as endothelial cell permeability, hepatocyte microvilli, and collagen layer filling in the Disse space were investigated. Moreover, the effects of microflow on the deformation of red blood cells (RBCs) in the sinusoidal cavity were discussed.

MATERIALS AND METHODS

Theoretical modeling

Hepatic sinusoid

A simplified hepatic sinusoid model with a defined size and geometry is illustrated in Fig. 1 *A*. The presence of endothelial cell layer segregates the sinusoid into three zones: the sinusoid cavity, endothelial cell layer, and Disse space. The height of the sinusoid cavity is H, thickness of endodermis is m_h, and width of the Disse space is D_h. The wall of the sinusoid model is considered the surface of hepatocytes, with a gap between the

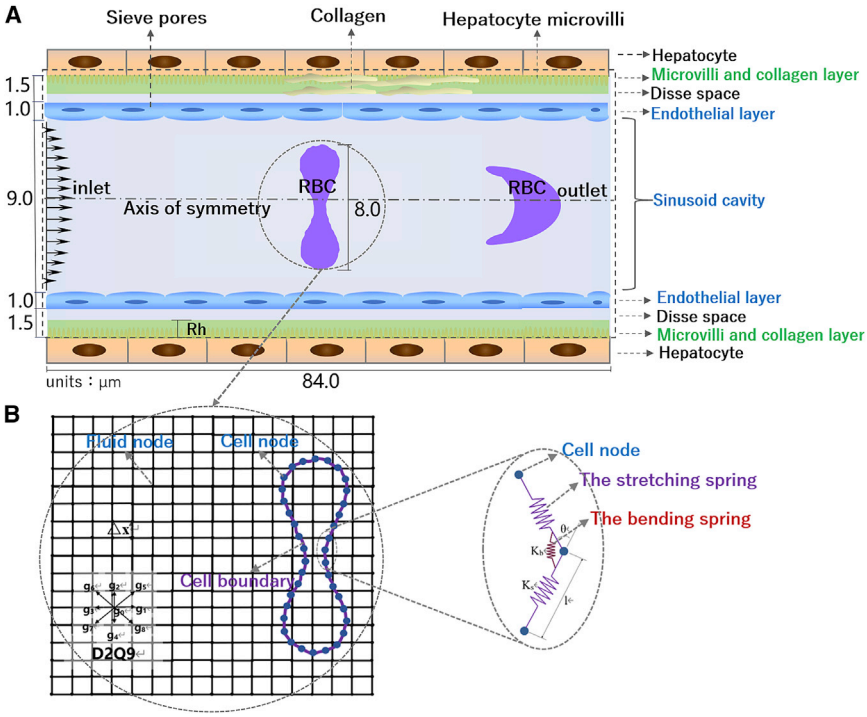

FIGURE 1 Mechanical model for a hepatic sinusoid and a red blood cell (RBC). (*A*) 2D schematic of a typical hepatic sinusoid. Four regions are segregated as a hepatocyte layer, a Disse space, an endothelium, and a sinusoidal cavity with an RBC embedded. (*B*) Coupled method of numerical calculations. D2Q9 model in LBM was used for flow calculation. Each flow field node has nine migration directions after each collision step. The fluid-solid coupling between RBC membrane and blood flow was calculated by IBM. Both IBM and LBM were coupled in calculations. Right panel elaborates the schematic of the mechanical model of an RBC. To see this figure in color, go online.

endothelial cell layer and hepatocytes that is filled with collagen when liver fibrosis occurs. Collagen adheres to the surface of hepatocytes and affects the blood flow in the Disse space, together with hepatocyte microvilli. Flow direction is set from left to right, and the inlet flow rate is set at a constant value u_0. The initial location of an RBC is set in the middle of the sinusoid cavity.

Endothelial layer

There are many sieve pores in the endothelial layer through which blood from the hepatic sinusoids flows into the Disse space (Fig. 1 *A*). The process of blood flow through the endothelial layer is similar to seepage; therefore, the endothelial layer is assumed to be a porous media layer. The flow in the porous media layer satisfies Darcy's law (18):

$$\nabla P = -\frac{\mu}{k}\mathbf{u}, \tag{1}$$

where $\mathbf{u}$ is the flow velocity, k is the permeability coefficient of the endothelial layer, and μ is the dynamic viscosity coefficient of plasma. P, which stands for pressure, represents the effects of external forces on blood flow to describe the percolation effect of the endothelium on blood flow.

Hepatocyte microvilli and collagen layer

The microsized Disse space, with numerous hepatocyte microvilli on the surface of hepatocytes (Fig. 1 *A*), can be considered as an irregular, rough surface to illustrate wall roughness effects on blood microflow. When the liver is fibrotic, a collagen layer formed by a large amount of collagen deposition in the Disse space (Fig. 1 *A*) aggravates the impact of the rough surface. For simplification, these hepatocyte microvilli and collagen layers (HMVCLs) are assumed to be porous, permeable medium layers with uniform thickness to unify the effects of surface roughness on blood flow (Fig. 1 *A*). Thus, the thickness of the permeable porous media layer is set to be R_h, and the seepage satisfies the following equation (18,19):

$$\mathbf{R} = -\frac{\mu}{k_r}\mathbf{u} - \frac{\beta}{\sqrt{k_r}}|\mathbf{u}|\mathbf{u}, \tag{2}$$

where k_r is the permeability coefficient of HMVCLs, β is related to the porosity of the permeable layer, and $\mathbf{R}$ is taken to be the external force on blood flow. Here, the surfaces of HMVCLs are assumed to be rougher and more irregular than those of the endothelial cell layer. Compared with Darcy's law seepage model, a nonlinear term is added in the Kleinstreuer's rough layer model of porous permeable media (19). To test the effects of surface roughness on blood flow, this nonlinear term was retained in these calculations. Because of the low flow velocity in the Disse space, the effect of this term was not significant.

RBCs

The RBC spring model proposed by Tsubota (20) was adopted for modeling RBC deformation. In brief, the cell membrane is considered to be composed of solid nodes, which are connected by three kinds of springs: stretch, bend, and area. The nodes are connected in turn and form a two-dimensional closed loop. The solid node of the membrane represents the position of the particle boundary (Fig. 1 *B*).

$$E_s = \frac{1}{2}K_s\sum_{i=1}^{N}\left(\frac{l_i - l_0}{l_0}\right)^2 (i = 1, 2, 3\ldots N). \tag{3}$$

$$E_b = \frac{1}{2}K_b\sum_{i=1}^{N}\tan^2\left(\frac{\theta_i - \theta_0}{2}\right) (i = 1, 2, 3\ldots N). \tag{4}$$

$$E_a = \frac{1}{2}K_a\left(\frac{a - a_0}{a_0}\right)^2. \tag{5}$$

$$\mathbf{f}_i = -\frac{\partial W}{\partial \mathbf{x}_i} = -\frac{\partial(E_s + E_b + E_a)}{\partial \mathbf{x}_i} (i = 1, 2, 3\ldots N). \tag{6}$$

Among these, E_s, E_b, and E_a represent three types of energy—stretching, bending, and area constraint, respectively—and K_s, K_b, and K_a represent the springing stiffnesses corresponding to those three energy terms. N represents the number of solid nodes of the cell membrane; l, θ, and a denote the distance between adjacent nodes, the angle of adjacent springs, and the cell model area, respectively. The subscript i is the serial number of the spring, and the subscript 0 is the initial values of the parameters, the corresponding equilibrium position of the springs, and $\mathbf{f}$ is the force on the node, which can be divided into x and y components, according to the principle of virtual work based on the total energy, W.

Numerical simulations

The immersed boundary method (IBM) coupled with the lattice Boltzmann method (LBM) was used to calculate microflow and cell deformation in the hepatic sinusoids. Herein, blood flow was calculated using LBM, and the RBC deformation was calculated using IBM, as shown in Fig. 1 *B*. LBM is a microscale method and applicable to conduct multi-interface fluid-solid coupling calculation for low-speed flow (21). Based on the original lattice Boltzmann equation, the effects of the endothelium, HMVCLs, and RBCs on blood flow were tested by introducing three additional force terms of P_i, R_i, and S_i into the following equation:

$$g_i(\mathbf{x}+\mathbf{c}_i\Delta t, t+\Delta t) - g_i(\mathbf{x},t) = -\frac{\Delta t}{\tau}[g_i(\mathbf{x},t) - g_i^{eq}(\mathbf{x},t)] + \Delta t\cdot P_i + \Delta t\cdot R_i + \Delta t\cdot S_i \quad (i = 0,1,2,3\ldots 8) \tag{7}$$

and

$$\mu_D = \mathbf{c}_s^2\left(\frac{\tau}{\Delta t} - 0.5\right)\Delta t, \tag{8}$$

where g_i is the distribution function for a particle with velocity $\mathbf{c}_i$ at position $\mathbf{x}$ at time t; $\mathbf{c}_i$ is the distribution function of migration distance along i^{th} direction per unit time, i.e., the migration velocity; g_i^{eq} is the equilibrium distribution function; Δt is the time increment; and τ is the relaxation time associated with blood viscosity (Eq. 8). μ_D is the kinematic viscosity of plasma. P_i, R_i, and S_i denote the force terms of the endothelial layer, HMVCL, and RBC membranes, respectively, along the i^{th} direction on the fluid nodes. Of note, Dacy's law was satisfied only in the endothelium region, and Kleinstreuer's model worked only in the HMVCL region. The continuity of pressure and velocity was also satisfied on the interfaces between endothelial layer and sinusoid cavity and the interfaces between HMVCL and the Disse space. Those two external source terms were assumed to be zero outside the regions of the endothelium and HMVCL. For the D2Q9 model, the migration speed is $\mathbf{c}_0 = (0, 0)$; $\mathbf{c}_i = \left(\cos\left(i-\frac{1}{2}\right), \sin\left(i-\frac{1}{2}\right)\right)\frac{\Delta x}{\Delta t}$; $(i = 1, 2, 3, 4)$; $\mathbf{c}_i = \left(\cos\left(i-\frac{9}{4}\right), \sin\left(i-\frac{9}{4}\right)\right)\sqrt{2}\,\frac{\Delta x}{\Delta t}$ $(i = 5, 6, 7, 8)$. Δx is the length of the lattice.

In Eq. 7, g_i^{eq}, P_i, R_i, and S_i are calculated using Eqs. 9, 10, 11, and 12:

$$g_i^{eq}(\mathbf{u},\rho) = \omega_i\rho\left[1 + \frac{\mathbf{c}_i\cdot\mathbf{u}}{c_s^2} + \frac{(\mathbf{c}_i\cdot\mathbf{u})^2}{2c_s^4} - \frac{\mathbf{u}\cdot\mathbf{u}}{c_s^2}\right], \tag{9}$$

$$P_i = \left(1-\frac{\Delta t}{2\tau}\right)\omega_i\left(\frac{\mathbf{c}_i-\mathbf{u}}{c_s^2} + \frac{\mathbf{c}_i\cdot\mathbf{u}}{c_s^4}\mathbf{c}_i\right)\cdot\mathbf{P}, \tag{10}$$

$$R_i = \left(1-\frac{\Delta t}{2\tau}\right)\omega_i\left(\frac{\mathbf{c}_i-\mathbf{u}}{c_s^2} + \frac{\mathbf{c}_i\cdot\mathbf{u}}{c_s^4}\mathbf{c}_i\right)\cdot\mathbf{R}, \tag{11}$$

and

$$S_i = \left(1-\frac{\Delta t}{2\tau}\right)\omega_i\left(\frac{\mathbf{c}_i-\mathbf{u}}{c_s^2} + \frac{\mathbf{c}_i\cdot\mathbf{u}}{c_s^4}\mathbf{c}_i\right)\cdot\mathbf{S}, \tag{12}$$

where $\mathbf{u}$ is the velocity of blood flow, the weights are given by $\omega_0 = 0.444$, $\omega_i = 0.111$ for $i = 1$–4, $\omega_i = 0.278$ for $i = 5$–8, c_s is the speed of sound, and $\mathbf{P}$ is the force of the endothelial layer on flow field (Eq. 1). $\mathbf{R}$ is the force exerted by HMVCL (Eq. 2). $\mathbf{S}$ is the force exerted by RBC membranes on the blood flow and is only considered in section 3.3. Subsequently, IBM was used to convert the force $\mathbf{f}$ of RBC membrane model into the force $\mathbf{S}$ on the flow field using the Dirichlet function:

$$\mathbf{S}(\mathbf{x}) = \sum_m D(\mathbf{x}-\mathbf{x}_m)\mathbf{f}(\mathbf{x}_m). \tag{13}$$

Here, $D(x)$ is the cosine Dirichlet function, and $\mathbf{x}$ and $\mathbf{x}_m$ are the positions of flowing fluid nodes and RBC membrane nodes, respectively.

After solving Eq. 7 to obtain the distribution function $g_i(\mathbf{x}, t)$, the macroscopic physical quantity density ρ, velocity $\mathbf{u}$, and pressure p of blood flow can be determined by the following equations:

$$\rho(\mathbf{x},\mathrm{t}) = \sum_i g_i(\mathbf{x},\mathrm{t}), \tag{14a}$$

$$\rho(\mathbf{x},\mathrm{t})\cdot\mathbf{u}(\mathbf{x},\mathrm{t}) = \sum_i g_i(\mathbf{x},\mathrm{t})\mathbf{c}_i + \frac{\Delta t}{2}\mathbf{P} + \frac{\Delta t}{2}\mathbf{R} + \frac{\Delta t}{2}\mathbf{S}, \tag{14b}$$

and

$$p = \rho c_s^2. \tag{14c}$$

The interactions between RBCs and blood flow are calculated using IBM. After the flow velocity in each node is obtained, the velocity of RBC membrane grid nodes is calculated using the Dirichlet function. The new position of the RBC membrane is calculated according to the velocity in each node $\mathbf{u}_{cell}$:

$$\mathbf{u}_{cell}(\mathbf{x}_m) = \sum D(\mathbf{x}-\mathbf{x}_m)\mathbf{u}(\mathbf{x}). \tag{15}$$

Overall, the numerical calculations using IBM-LBM can be summarized as follows: 1) calculating the body force on each node of flow field given by the RBC membrane (Eqs. 6 and 13), 2) solving the flow field and obtaining flow velocity (Eqs. 7, 8, 9, 10, 11, 12, 14a, 14b, and 14c), 3) calculating the new velocity in each RBC membrane node (Eq. 15) and updating the positions of RBC membrane nodes, and 4) returning to step 1 and repeating

until the preset convergence criteria are met. With this approach, the coupling effect of blood flow and RBC membrane is evaluated.

Parameter setting and data analysis

The surface of hepatocytes was set as no-slip boundary conditions. The LBM adopted in this work was performed using a dimensionless method for governing equations, boundary conditions, and meshes. Here, the unit grid length $\Delta x = \Delta y = 1$, where one grid length corresponds to the physical unit of 0.1 μm, and the time step $\Delta t = 1$, where one time step corresponds to the actual physical time of 3.334×10^{-9} s. The inlet flow rate was constant at 2.54×10^{-6} mL/min, which was converted based on two-dimensional (2D) flow velocity at a given Reynolds number, *Re*, of 0.01. In fact, assuming that the geometry for this 2D model was a circular tube with a diameter H_{inlet}, the flow rate with a three-dimensional (3D) characterized size of H_{inlet} can be calculated as $Q = \pi(H_{inlet}/2)^2 u_{inlet}$ when 2D velocity $u_{inlet} = 1333.3$ μm/s. The mass-modified outlet boundary of LBM for the outlet was used to ensure the conservation of mass flow at the outlet and inlet. The flow velocity at the outlet boundary was calculated using Eqs. 16a and 16b,

$$u_x(N_x, j) = \zeta \cdot u_x(N_x - 1, j) \tag{16a}$$

and

$$u_y(N_x, j) = 0.0, \tag{16b}$$

where (N_x, j) was the node on the outlet boundary and $(N_x - 1, j)$ was the adjacent fluid node. ζ was the mass-modified coefficient, calculated by Eq. 17:

$$\zeta = \frac{\sum_j \rho(1,j) u_x(1,j) \Delta y}{\sum_j \rho(N_x,j) u_x(N_x - 1,j) \Delta y}. \tag{17}$$

The process of mass-modified outlet boundary was set as follows: 1) calculating the mass-modified coefficient ζ by Eq. 17 and 2) calculating the flow velocity at the outlet boundary by Eqs. 16a and 16b. Please refer to the details for LBM mass-modified outlet boundary conditions in the literature (22). Plasma was assumed to be an incompressible Newtonian fluid with a viscosity of 1.2 cP and a density of 1000 kg/m^3. The relaxation time τ was set to be 1.7 based on Eq. 8 in (14) in an in vitro liver chip model, and the porous membrane permeability coefficient was assigned to be 10^{-16} m^2 according to the experimental and numerical results in the same literature. Thus, it was assumed that the permeability coefficient, *k*, of the endothelial layer was 10^{-16}–10^{-13} m^2 (14). A higher permeability coefficient denotes more sieve pores in the endothelial cells. Meanwhile, the hydraulic resistivity of the macromolecular layer adjacent to the endothelium was assigned to be $\sim 10^8$ dyn · s/cm^4 in the literature (23), from which the endothelium permeability coefficient was estimated to be $\sim 10^{-14}$ m^2. Therefore, the permeability coefficient of HMVCL, k_r, was set on a scale of 10^{-16}–10^{-14} m^2. The higher the permeability coefficient, the greater the porosity of HMVCL, indicating that the collagen filling is sparse. R_h-values of the thickness of HMVCL range from 0.2 to 1.0 μm. A thick layer means a large amount of collagen deposition in the Disse space (for parameters see Table 1).

A FORTRAN program was in-house coded to perform numerical simulations, and its accuracy and reliability were verified by calculating the typical Poiseuille pressure-driven flow field and deformation dynamics of RBCs in a single channel. The convergence criterion for the steady state of the flow was given for the relative error of velocity being less than 10^{-6}. Data indicated that the resultant error between numerical calculations and theoretical solution of Poiseuille flow was <1%. Furthermore, in the IBM, the distance between solid nodes (dynamic mesh size Δs) and the mesh size of flow field (static mesh size Δx) satisfied $\Delta s < \Delta x/2$. Mesh convergence was tested by setting the node number of RBCs to be 199, 299, and 399, respectively. RBC deformation was then calculated in a single channel and the results were compared with those in the literature (24), yielding the corresponding errors were 6.89, 1.24, and 1.16%, respectively. Thus, the mesh with 299 nodes was selected to balance both high precision and high computational efficiency. Total 1.0×10^4–2.0×10^4 and 1.0×10^7–1.0×10^8 time steps were set for calculating blood flow in the absence and presence of RBCs, respectively.

TABLE 1 Relevant parameters used in the calculation

Parameters	Values
Density ρ	1000 kg/m^3
Kinematic viscosity μ	1.2 cp (4)
Re	0.01
Relaxation time $\tau/\Delta t$	1.7
Permeability of endothelial cell laye *k*	10^{-16}–10^{-13} m^2 (estimated by (14))
Permeability of HMVCL k_r	10^{-16}–10^{-14} m^2 (estimated by (22))
Coefficient β	5.5×10^2 kg/m^3 (19)
Stretching stiffness K_s	3.6×10^{-17} N m (20,23)
Bending stiffness K_b	1.44×10^{-19} N m (20,23)
Area stiffness K_a	3.6×10^{-14} N m (20,23)
Initial area of RBC a_0	1.425×10^{-11} m^2

Data availability

The data that support the findings of this study are available within the article and the references cited.

RESULTS

Flow velocity and flow rate distributions in the hepatic sinusoid

A hepatic sinusoid can be divided into two parts, the sinusoid cavity and Disse space, which are separated by an endothelial layer. When hepatic sinusoid lesions occur, the permeability of the endothelial cell layer is altered, which causes a change in the flow velocity in the sinusoid cavity and Disse space. When the hepatic sinusoid is fibrotic, the collagen filling in the Disse space further affects the blood flow. Therefore, we first calculated the flow field in the hepatic sinusoid without RBCs and quantified the basic characteristics of microflow. The distribution of flow velocity is shown in Fig. 2 *A*, in which the permeability coefficient of the endothelial layer was 2.5×10^{-16} m^2 and the thickness of HMVCL was zero. Evidently, fluid flow in the sinusoid cavity is laminar, and flow velocity in the endothelial layer and Disse space regions is very low compared with that in the sinusoid cavity. Subsequently, we varied the permeability coefficient of the endothelial layer, and the corresponding flow-velocity profiles in the hepatic sinusoid are shown in Fig. 2 *B*. Because the endothelium was assumed to be a porous media layer, both the velocities *u* and *v* in the *x* and *y* directions were affected by the permeability coefficient. When the permeability coefficient was greater than

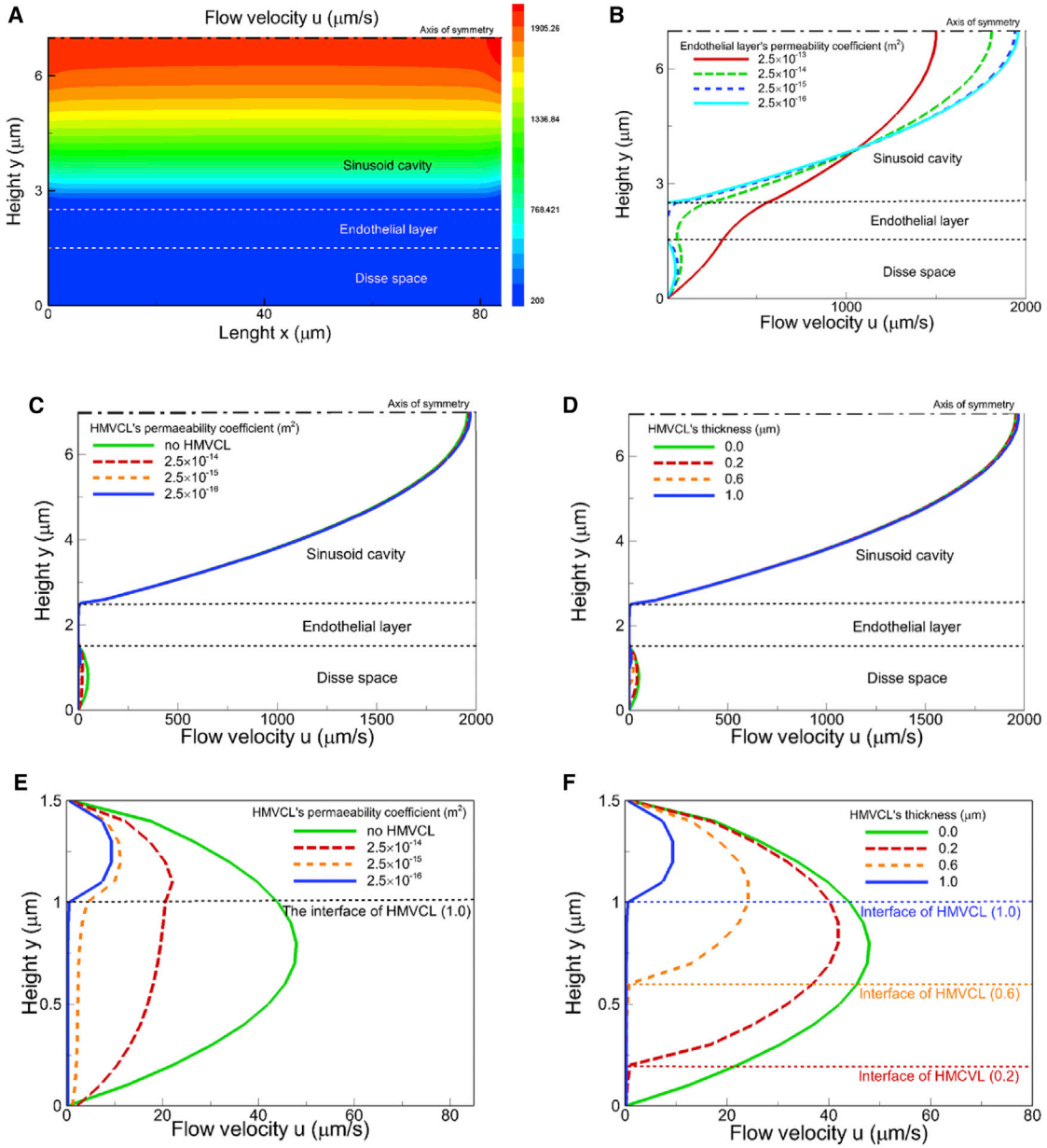

FIGURE 2 Fluid velocity analysis inside the sinusoid. (*A*) Flow-velocity distribution in the half plane of a hepatic sinusoid. (*B–D*) Profiles of flow velocity in the entire sinusoid, with varied endothelial permeability coefficients when the thickness of HMVCL in the Disse space was set to be zero (*B*) or 1.0 μm (*C*) or with varied HMVCL thicknesses when the permeability coefficient of HMVCL was set to be 2.5×10^{-16} m^2 (*D*). (*E* and *F*) Profiles of flow velocity in the Disse space, with varied permeability coefficients of HMVCL when the HMVCL thickness was set to be 1.0 μm (*E*) or with varied HMVCL thicknesses when the permeability coefficient of HMVCL was set to be 2.5×10^{-16} m^2 (*F*). To see this figure in color, go online.

10^{-14} m^2, u was more than two orders of magnitude larger than v, suggesting that u was dominated in the endothelium. With the decrease of endothelial permeability coefficient, u decreased sharply but v increased gradually. When the endothelial permeability was reduced to 10^{-16} m^2, u was close to zero. Despite the fact that v became larger than u in this case, v was still small. Thus, we focused on the change of the velocity u below. In Fig. 2 *B*, we can see that, with an increase in the endothelial permeability coefficient, flow velocity decreased significantly in the sinusoid cavity, increased in the Disse space, increased more rapidly near the endothelial surface, and gradually reached the maximal value in the Disse space. When the permeability coefficient of the endothelial layer ranged from 2.5×10^{-16} to 2.5×10^{-13} m^2, the maximal flow velocity in the Disse space increased 6.8-fold, and the flow velocity in the sinusoid cavity decreased 0.8-fold. Therefore, the permeability of the endothelial layer had a significant impact on the flow in the hepatic sinusoid and governed the flow-velocity distribution in the sinusoid cavity and Disse space. With an increase in endothelial

permeability, the maximal velocity in the sinusoidal cavity decreased gradually, maintaining a parabolic shape; however, the velocity in the Disse space was no longer parabolic but had greater velocity near the endothelial layer.

The effect of the HMVCL on flow field in the Disse space was further investigated. By varying the permeability coefficient and thickness of the HMVCL in the Disse space at a constant endothelial layer permeability coefficient ($k = 2.5 \times 10^{-16}$ m^2), the flow-velocity profiles obtained are shown in Fig. 2, *C and D*. It was evident that the flow velocity varied significantly in the Disse space, but only minor changes were noted in the sinusoid cavity. Enlarging those flow rate profiles in the Disse space in Fig. 2, *C and D* resulted in velocity profiles with varied permeability coefficients (Fig. 2 *E*) and thickness (Fig. 2 *F*) of HMVCLs in the Disse space. It can be observed that HMVCLs segregate the Disse space into two flow regions. In the HMVCL, the flow velocity is low, and the flow is gentle. When its permeability coefficient is decreased and thickness is increased, flow resistance increased in the HMVCL, and flow velocity decreased in the Disse space. Setting the permeability coefficient as 2.5×10^{-16} m^2 and thickness as 1 μm, the maximal flow velocity was decreased by 80.5% in the Disse space. Therefore, the characteristics of the HMVCL significantly affect flow velocity in the Disse space; however, it has little impact in the sinusoid cavity.

The flow rate in the Disse space was further analyzed. With varied permeability coefficient and thickness of the HMVCL, flow rate in the Disse space was altered remarkably, and permeability coefficients of the endothelial layer were also varied (Fig. 3). As can be observed from Fig. 3, *A–D*, the Disse space flow rate was lower when the HMVCLs were thicker and their permeability coefficient was lower. Table 2 shows the magnitude of flow rate reduction in the Disse space compared with that in the absence of HMVCLs, in which the flow rate reduction was 90.0% at most. Thus, HMVCLs significantly abolish fluid flow in the Disse space when their thickness is high and permeability is low. Furthermore, the flow in the Disse space was regulated by endothelial permeability. The larger the endothelial permeability coefficient, the larger the Disse space flow. Typically, when the endothelial permeability coefficient was 2.5×10^{-13} m^2, the maximal reduction of flow rate was 83.0%. Therefore, endothelial permeability is another key factor affecting Disse space flow, and the flow in the HMVCL decreases faster at high endothelial permeability.

Shear stress of blood flow on the surfaces of hepatocytes and endothelium

The mechanical signals of hepatocytes arise primarily from the blood flow in the Disse space. The microvilli on the surface of hepatocytes exert remarkable impacts on the blood flow in vivo primarily because of the confined Disse space. Furthermore, in a fibrotic or cirrhotic liver, the collagen deposit in the Disse space affects the blood flow. Next, we tested the effects of HMVCLs on blood flow and shear stress in the Disse space. Fig. 4 *A* shows the flow shear stress distribution in the hepatic sinusoid at a given HMVCL thickness of 1 μm. Inflection points were observed on the upper and lower interfaces of the endothelium, as well as on the interface of

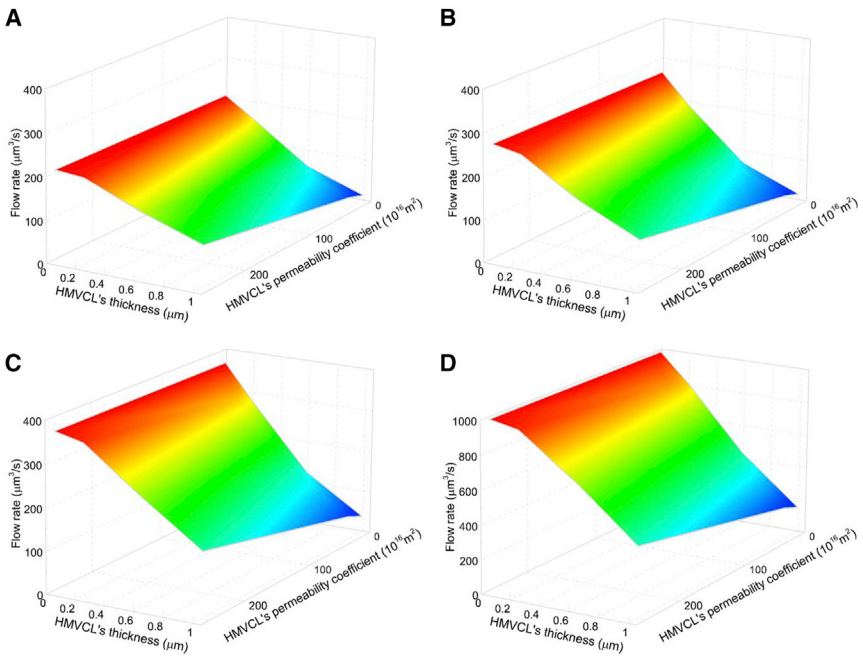

FIGURE 3 Flow rate analysis in the Disse space. (*A–D*) Distributions of flow rate with varied HMVCL permeability coefficients and thicknesses when the endothelial permeability coefficient was set to be 2.5×10^{-16} m^2 (*A*) or 2.5×10^{-15} m^2 (*B*) or 2.5×10^{-14} m^2 (*C*) or 2.5×10^{-13} m^2 (*D*). To see this figure in color, go online.

TABLE 2 Disse space flow rate with varied permeability coefficients and thicknesses of HMVCL

Flow reduction (%)		Thickness of HMVCL		
		0.2 μm	0.6 μm	1.0 μm
Permeability coefficient of HMVCL	2.5×10^{-14} m^2	3.0	30.0	52.0
	2.5×10^{-15} m^2	16.0	62.0	87.0
	2.5×10^{-16} m^2	23.0	69.0	93.0

the HMVCL, indicating the force exchange between blood flow and endothelial cells. Fig. 4 *B* depicts the source of flow shear stress exerted on the surface of hepatocytes, which can be divided into two parts. The first part is derived from blood flow that is transmitted to the hepatocytes via HMVCLs and is related to the value of shear stress on the surface of the HMVCL (*red arrows*). The second part is derived from blood flow penetrating through HMVCLs and acts directly on the surface of hepatocytes (*blue arrows*). Because of the osmotic effect of the HMVCL, the blood flow from the second source is greatly reduced, and hence, shear stress on the hepatocytes is quite low compared with that of the first source (Fig. 4 *A*). Thus, we focused on the shear stress on the surface of HMVCLs at varying endothelial permeability coefficients and HMVCL thicknesses. When the permeability coefficient was low, shear stress decreased with the increase in thickness, typically yielding a shear stress reduction of 58.9% at the permeability of 2.5×1.0^{-16} m^2 (*red line*). When the coefficient was high, shear stress increased with the increase in thickness, typically yielding a shear stress increase of 18.9% at the permeability of 2.5×1.0^{-13} m^2 (*blue line*) (Fig. 4 *C*). The impact of HMVCL thickness on the shear stress is opposite when the endothelial permeability coefficient is varied and the change of the shear stress at the surface is biphasic. In contrast, no obvious biphasic pattern was found upon altering the HMVCL permeability coefficient for

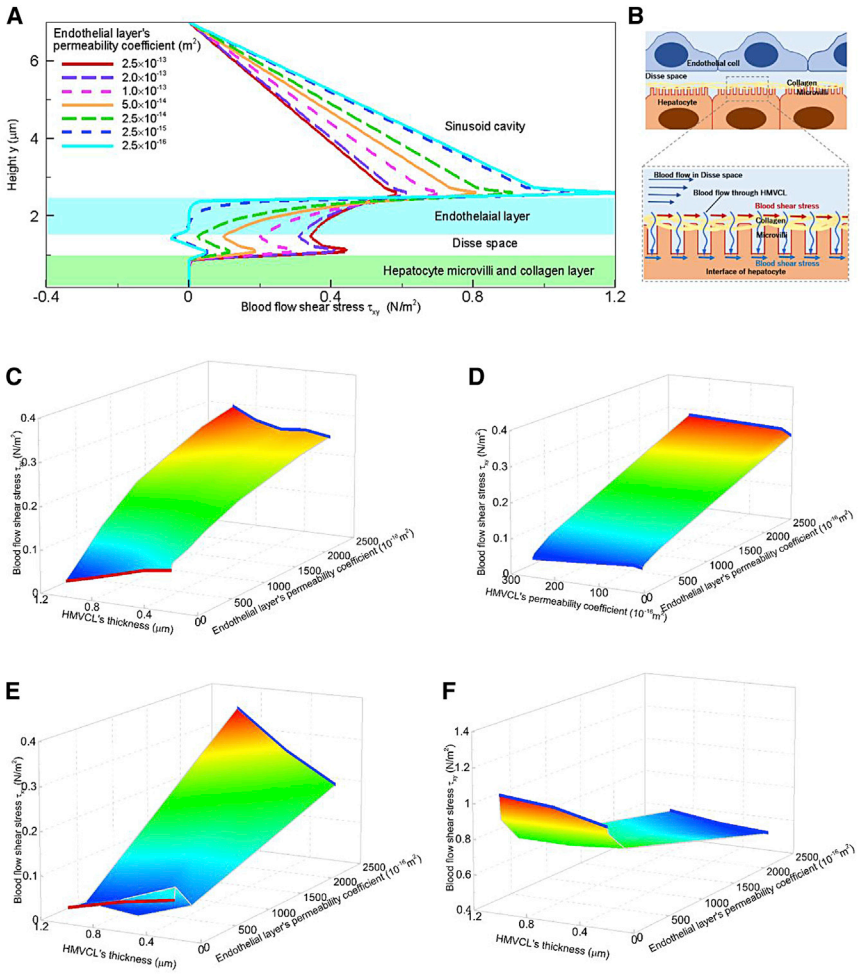

FIGURE 4 Flow shear stress analysis inside the sinusoid. (*A*) Profiles of flow shear stress along the *y* direction with varied endothelial permeability coefficients. (*B*) Schematic of the two possible sources of blood flow to exert shear stresses on the hepatocytes. (*C* and *D*) Distributions of shear stress on the HMVCL surface with varied endothelial permeability coefficients and HMVCL thicknesses when HMVCL permeability coefficient was set to be 2.5×10^{-16} m^2 (*C*) or with varied endothelial and HMVCL permeability coefficients when HMVCL thickness was set to be 0.6 μm (*D*). (*E* and *F*) Distributions of shear stress on the lower (*E*) or upper (*F*) surface of the endothelium with varied endothelial permeability coefficients and HMVCL thicknesses when HMVCL permeability coefficient was set to be 2.5×10^{-16} m^2. To see this figure in color, go online.

regulating the shear stress on the HMVCL surface (Fig. 4 *D*). Thus, varying HMVCL thickness affects the shear stress on their surface, and alteration of shear stress produces a biphasic pattern with varying endothelial permeability. Blood shear stress is directly related to velocity gradient. Velocity gradient on the HMVCL surface is affected by two factors—the size and velocity value of the Disse space. When the endothelial permeability was low, flow velocity in the Disse space was parabolic and low. As HMVCL thickness increased, flow velocity tended to become lower, thereby reducing shear stress. When endothelial permeability was high, flow velocity was high and no longer parabolic. As HMVCL thickness increased, flow velocity tended to become higher, thereby increasing shear stress. However, when HMVCL permeability increased, flow at the interfacial surface of the HMVCL increased to a greater degree than the increase in the flow between the endothelial layer and the HMVCL regardless of whether the velocity was parabolic, which lowered the flow-velocity gradient and reduced the shear stress. Thus, no biphasic pattern was exhibited. Further, we calculated flow shear stress on the lower (Fig. 4 *E*) and upper (Fig. 4 *F*) endothelial surfaces. A biphasic distribution of shear stress was presented on the lower surface but not on the upper surface. Typically, the shear stress on the lower surface of the endothelium decreased by 55.2% at the endothelial permeability coefficient of 2.5×1.0^{-16} m^2; however, it increased by 84.0% at the coefficient of 2.5×1.0^{-13} m^2. Collectively, shear stress on the lower surface of the endothelium and on the upper surface of the HMVCL produce a biphasic pattern regulated by HMVCL thickness and endothelial permeability in the Disse space. As endothelial permeability increased, flow in the Disse space became no longer parabolic, and flow at the lower surface of the endothelium tended to slip, which lowered the flow-velocity gradient and reduced the shear stress. When endothelial permeability continued to increase, flow at the lower surface of the endothelium gradually reached the maximal value in the Disse space, implying that shear stress increased as the velocity gradient increased.

To further elucidate the physical rationale behind this biphasic pattern of shear stress in the Disse space, theoretical analysis was also conducted. Assuming that the thickness of the endothelium is very low, an approximate theoretical solution for flow velocity in the hepatic sinusoids is obtained, as shown in Eqs. 18 and 19 (see Supporting materials and methods, Appendix A for details). Briefly, the maximal flow velocity in sinusoid cavity is approximated as u_{max} when the endothelial permeability coefficient is sufficiently high:

$$u_{max} = \frac{1}{8\mu}\frac{\Delta P}{\Delta x}m^2 = \frac{3}{2}\frac{Q}{m}, \tag{18}$$

where m is the size of the sinusoid cavity and Disse space (both are integrated into a single variable in the analysis), P is the flow pressure, and Q is the flow rate. The higher the HMVCL thickness, the smaller the size of the Disse space, and the smaller the m value is, indicating that u_{max} increases when Q remains unchanged. When flow-velocity gradient increases, shear stress increases accordingly. At a low endothelial permeability coefficient, the flow rate in the Disse space meets the following requirements:

$$u_2 \sim C_2 \times D_h^2 = \left(\frac{12\mu Q}{\mathrm{H}^3 + D_h^3 + 3b \times D_h^2} - \frac{1}{1 + \left(1 + \frac{3b}{D_h}\right)^{\frac{1}{h^3}}} \times \frac{2\mu}{k}\frac{m_h}{\overline{v}}{n} \right) \times D_h^2, \tag{19}$$

where u_2 is the flow velocity in the Disse space, D_h is the size of the Disse space, and h is H/D_h where H is the size of the sinusoid cavity and b is the slip length. D_h decreases with increase in the thickness of the HMVCL because h greatly increases at $D_h << H$. The term $H^3 + {D_h}^3 + 3b{D_h}^2$ changes slightly as a result of $D_h << H$; thus, the term in the left-hand side in the bracket of Eq. 19 does not change much. Only the term on the right-hand side increases, leading to a decrease in the total bracketed term and causing decrease in u_2 and shear stress accordingly. The comparisons between theoretical and numerical solutions are shown in Fig. 5. Typically, the shear stress decreased by 69.0% at an endothelial permeability coefficient of 2.5×10^{-16} m^2; however, it increased by 27.4% at an endothelial permeability coefficient of 2.5×10^{-13} m^2, consistent with the numerical simulations and confirming the rationality of the biphasic pattern of shear stress in the Disse space.

Deformation index and deformation rate of RBCs

The movement of RBCs in the hepatic sinusoids is related to oxygen transport and vascular obstruction; hence, RBCs are ideal model cells for understanding alterations in flow-driven cell movement in the sinusoid cavity. Fig. 6 *A* shows the deformation trajectories of RBCs in the sinusoid when the

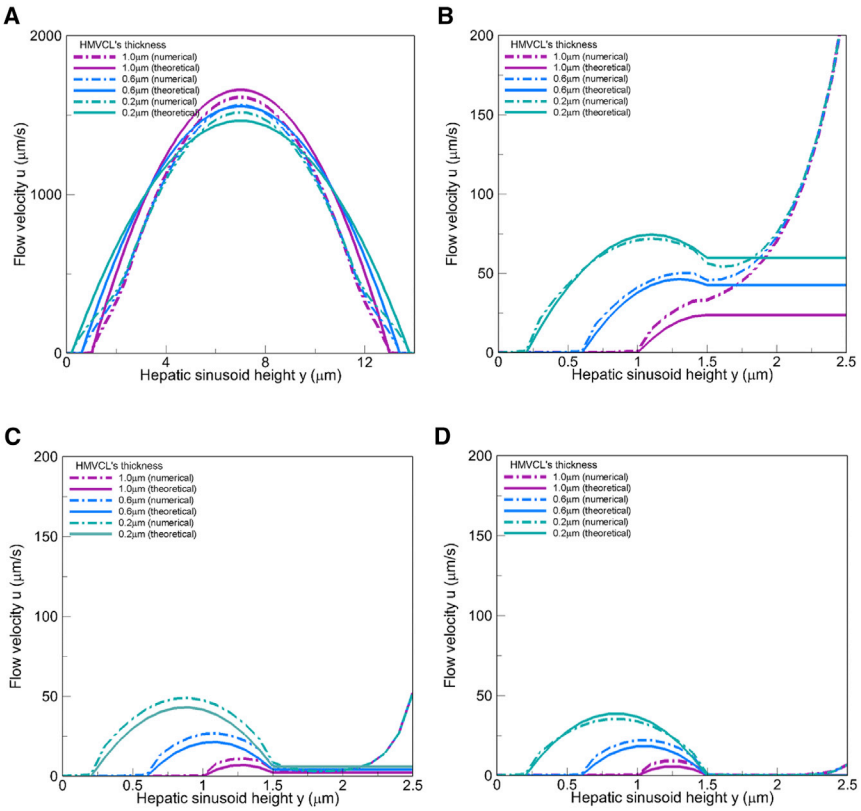

FIGURE 5 Comparisons between approximated theoretical solutions and numerical calculations of flow velocity profiles inside the sinusoid. (*A–D*) The data are presented on varied HMVCL thickness when the endothelial permeability coefficient was set to be 2.5×10^{-13} m^2 (*A*), 2.5×10^{-14} m^2 (*B*), 2.5×10^{-15} m^2 (*C*), or 2.5×10^{-16} m^2 (*D*). To see this figure in color, go online.

thickness of HMVCL was zero. RBC morphology changed from an initial double-concave butterfly shape to a parachute-dropping shape, and the variations in endothelial permeability significantly affected the deformation capability of RBCs. The lower the endothelial permeability coefficient, the more protruded the RBC front and the sharper the RBC tails. A deformation index was introduced for quantifying cellular shape, defined as the maximal size of RBCs along the x direction divided by the maximal size along the y direction and presented in Fig. 6 *B*, with different colors representing varied endothelial permeability coefficients. The greater the permeability coefficient, the lower the cellular deformation index. Typically, at $x = 60\,\mu$m, the index decreased by 26.7% from the lowest to highest permeability coefficient, which is attributed to the changes in flow velocity in the hepatic sinusoid (cf. Fig. 6 *B*).

RBC deformation rate can also be obtained by deriving the deformation index with respect to time, as shown in Fig. 6, *C–F* to illustrate the time courses of deformation rate with varied HMVCL thicknesses. The rate increases rapidly at the initial deformation stage, decreases gradually after reaching the peak, and then fluctuates in a stable interval. The higher the endothelial permeability coefficients, the lower the initial deformation rate, typically yielding a 47.1% reduction of the rate from the highest to lowest permeability coefficient at zero thickness of the HMVCL. It should be mentioned that the rapid increase of RBC deformation index in the initial stage of RBC deformation is partially induced by the initial shape of RBC. After RBC deformation is stabilized far beyond the peak, the rate did not differ significantly (i.e., >0.03 s), which means the cell deformation process was in the stable stage after $t = 0.03$ s. In other words, RBC deformation index varied greatly in the stable stage at varied endothelial layer permeability, whereas deformation rates presented little differences, indicating that RBC deformation did not change significantly. It was likely no effects of initial cell equilibrium shape existed in this stable stage of cell deformation. As can be seen from Fig. 6, *C–F*, cell deformation rate fluctuated up and down at this stage and gradually flattened out, and the larger the endothelial permeability coefficient, the more flattened the cell deformation rate, suggesting that the cell deformation was more stable when the endothelial permeability coefficient was larger. Moreover, endothelial permeability negatively regulates initial RBC deformation capabilities; however, HMVCL thickness has little effects on RBC deformation. This is biologically significant in liver fibrosis, in which endothelial capillarization tends to significantly affect RBC deformation in the sinusoidal cavity via modification of endothelial permeability, whereas collagen filling appears not to occur when the size of the Disse space remain unchanged.

Liver chip flow-velocity migration

The aforementioned numerical calculations can also be applied to optimize fluid dynamics in the design of

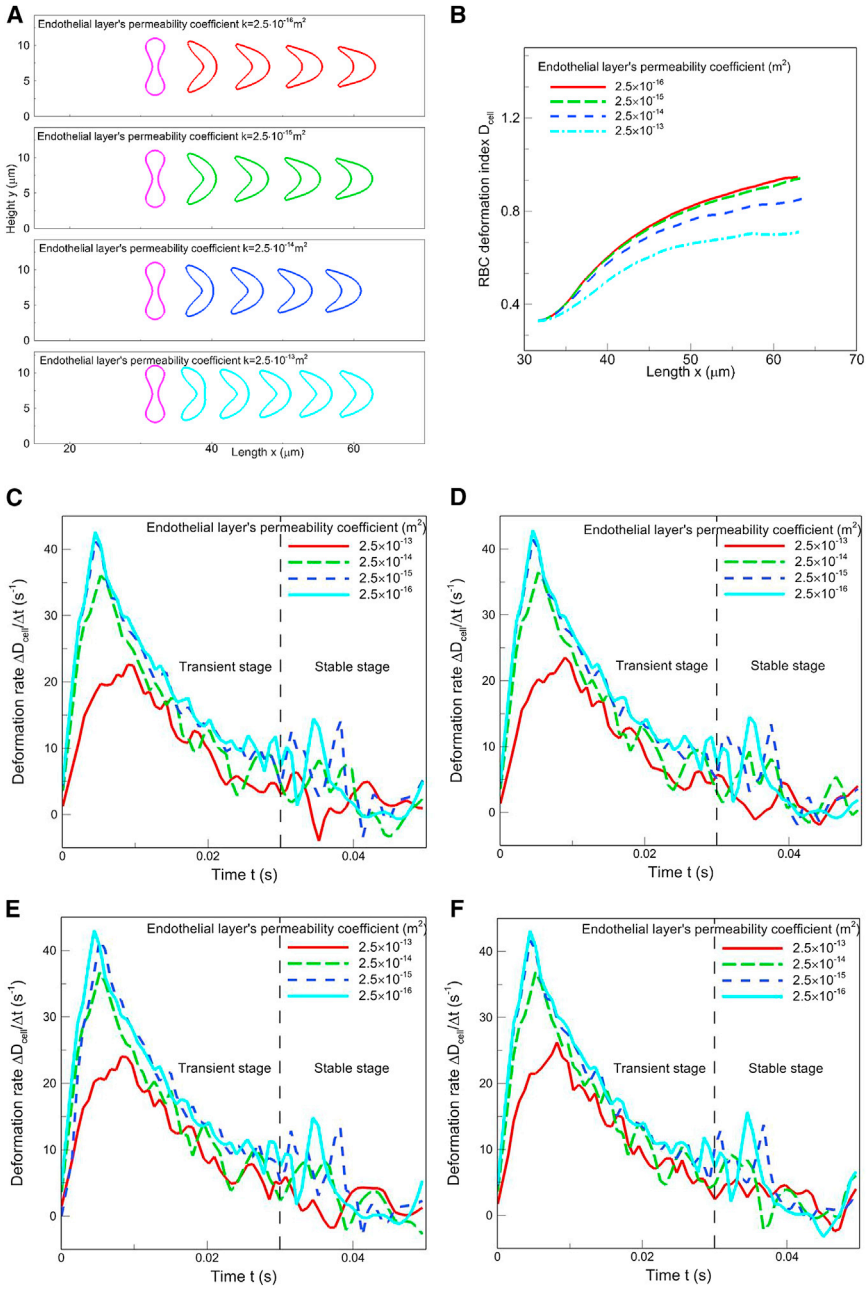

FIGURE 6 RBC deformation analysis in the sinusoidal cavity. (*A* and *B*) Typical snapshots of RBC morphology (*A*) or RBC deformation index (*B*) along the *x* direction with varied endothelial permeability coefficient when the HMVCL thickness was set to be zero. (*C–F*) Time courses of RBC deformation rate (i.e., deformation index with respect to time) with varied endothelial permeability coefficient of the endodermis when the HMVCL thickness was set to be zero (*C*), 0.2 (*D*), 0.6 (*E*), or 1.0 μm (*F*). To see this figure in color, go online.

in vitro liver chips or organoids. In one of our previous studies involving a double-channel liver sinusoidal chip, flow-velocity distributions were measured experimentally and calculated numerically (14). Interestingly, all of the measured points were concentrated on the side far away from the bottom wall of the lower channel, presumably because of the contributions of wall roughness to the lower velocity near the wall, leading to fewer experimental data points. To test this hypothesis, a 2D flow field model of this liver sinusoidal chip was established to evaluate the impacts of the lower-channel wall roughness on microflow (Fig. 7 *A*). The model is divided into two channels separated by a porous permeable medium layer. The fluid flows into the lower channel through the permeable layer from the upper entrance and flows out from the upper outlet. The inlet was set at a constant flow-velocity boundary condition, and the wall velocity has no slip. The flow rate was set to be consistent with the parameters used previously, in which the shear force on the wall of the upper channel was 0.1 dyne · cm^2 (14). Taking the roughness effect of the bottom wall of the lower channel into account, Mala's roughness-viscosity coefficient correction model was adopted (Eq. 20) (25).

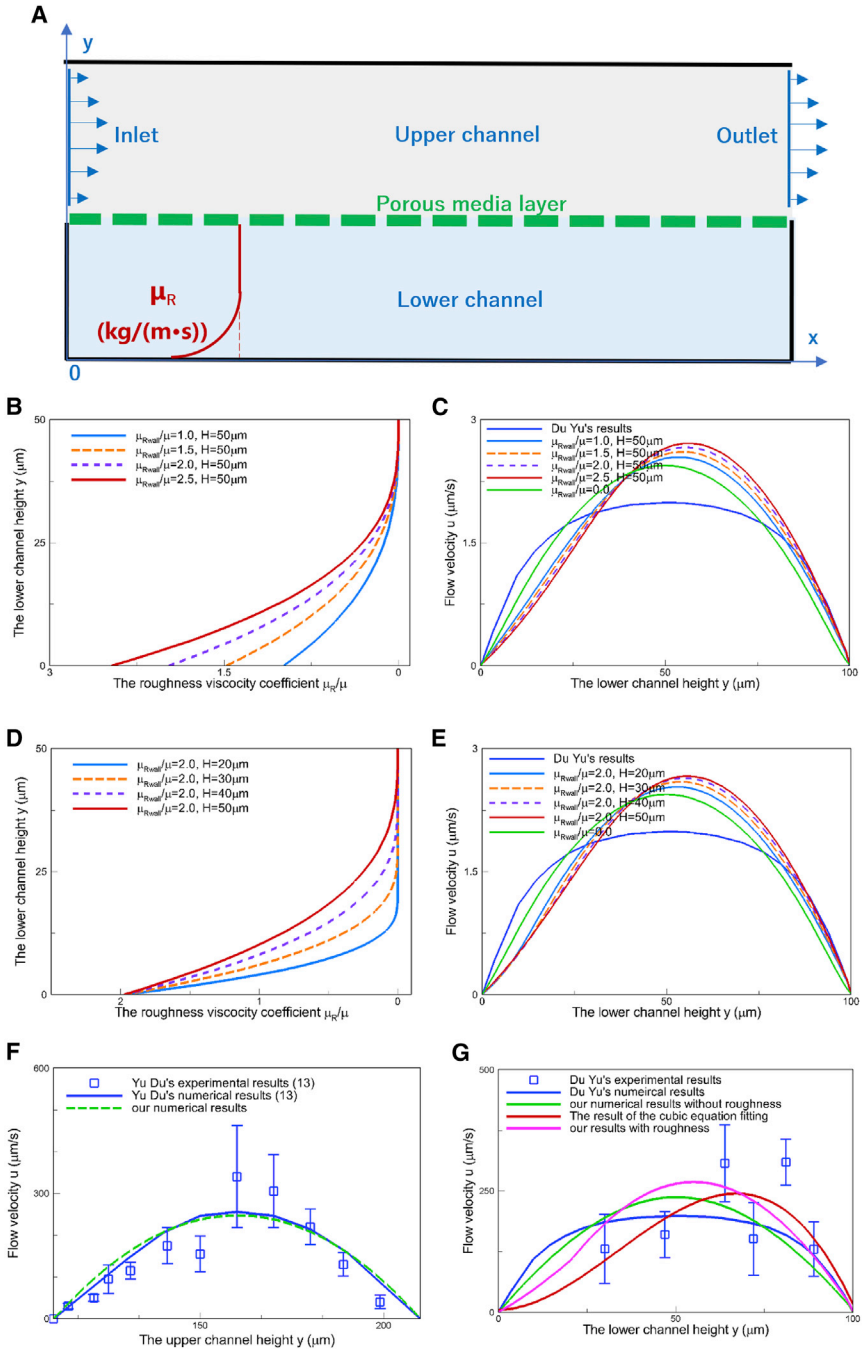

FIGURE 7 Comparisons between experimental data and numerical calculations of flow-velocity profiles inside the sinusoid. (*A*) Schematic of 2D liver sinusoidal chip used for estimating the roughness-viscosity coefficient. (*B* and *D*) Profiles of modified viscosity coefficients along the *y* direction, in which the coefficients at the wall surface ($y = 0$) are different and tend to 0 at the same height of the channel (*B*) or the values are same at $y = 0$ and approach 0 at the different heights of the channel (*D*). (*C* and *E*) Profiles of flow velocity in the lower chamber with varied viscosity coefficients shown in (*B*) and (*D*), respectively. (*F* and *G*) Comparisons of flow-velocity profiles in the upper (*F*) or lower (*G*) channel of liver sinusoidal chip. Previous data (*points*) and calculations (*blue lines*) were adopted from the literature (14). To see this figure in color, go online.

$$\mu_R = \mathrm{A} \times \rho \times u_{Rh} \times (H - y)\left(1 - \exp\left(-\frac{u_{Rh}}{u} \times \frac{(H - y)}{2H}\right)\right)^2 \quad (20)$$

and

$$\mu_{\mathrm{whole}} = \mu + \mu_R, \quad (21)$$

where μ_{R} represents the increase in the roughness-viscosity coefficient caused by the wall surface, implying that an increase in μ_{R} means an increase in wall roughness and its resistance to flow and the effect of wall roughness disappears when $\mu_{\mathrm{R}} = 0$. y is the distance of a point in the flow field from the wall surface. A is the coefficient of the roughness-viscosity function. ρ is the fluid density, and μ is the viscosity coefficient of the flow field at the center region. u_{Rh} represents the velocity of the flow field at a point R_{h}

units away from the wall, where R_h is the thickness of the rough layer. H denotes the correction range of the viscosity coefficient, and μ_{whole} denotes the final viscosity coefficient of the flow field.

To test the influence of the roughness-viscosity coefficient on flow velocity in the lower channel, multiple viscosity coefficients were obtained by systematically varying the μ_{Rwall}/μ-value at a given height of the lower channel, H (Fig. 7 *B*), or the H-value at a given μ_{Rwall}/μ (Fig. 7 *D*). The corresponding flow rate profiles are shown in Fig. 7, *C and E*, in which the maximal velocity in the lower channel is shifted away from the wall. The maximal offset yielded up to 14.0% (Table 3), mainly because of the rough-wall-induced increase of the flow resistance near the wall, which reduces the velocity near the wall and increases the velocity far from the wall at a constant flow rate, resulting in the shifting of the entire flow-velocity profile. Comparisons indicated that the calculated velocity profiles in the upper channel are consistent with experimental results (14) (Fig. 7 *F*). By contrast, the velocity profiles in the lower channel demonstrated slight differences from measurements reported in the literature (14) and the calculations in this work (Fig. 7 *G*). To estimate the relative errors, the experimental data (*points*) were refitted using a unitary cubic function (*red line*), yielding the fitting error of 27.2%. Moreover, the average error estimated from this fitting curve was 47.0 and 81.1% relative to our calculations with and without considering wall roughness, respectively. Both of these error values are lower than those of previous calculations (99.8%). Because both calculations that do not consider wall roughness have similar error values (81.1 and 99.8%) and remarkably lower accuracy than calculations in the presence of wall roughness, these comparisons further confirmed the necessity of considering wall roughness in calculating flow velocity, especially in the lower channel.

DISCUSSION

One of the major mechanical signals exerted on hepatocytes is derived primarily from the blood flow in the Disse space. The goal of this work was to elucidate how the existence of sinusoidal endothelial and collagen layers regulates the fluid dynamics of blood flow inside the hepatic sinusoids. A hepatic sinusoid model physiologically mimicking the hepatic sinusoid was established with an endothelial layer, HMVCL, and a Disse space. Three new source terms were introduced into the original IBM coupled with LBM, facilitating investigation of the effects of endothelial layer permeability, HMVCL resistance, and erythrocyte deformation on hepatic sinusoid microflow. Under physiological conditions, flow-velocity distribution maintained a parabolic shape in the sinusoidal cavity, and the maximal velocity decreased gradually with increased endothelial permeability. In contrast, velocity distribution in the Disse space became no longer parabolic, and higher velocities were presented near the wall of the endothelial layer. For comparison, the ratio of blood flow velocity through the fenestration of the sinusoid to flow velocity in the sinusoidal cavity was found to be 1.7–3.3% (15). In our results, the ratio of flow velocity through the Disse space to that in the sinusoidal cavity was 2.5–4.0% when the endothelial permeability was lower than 2.5×10^{-14} m^2, which is close to those in the literature. In liver fibrosis, a large amount of collagen is deposited in the Disse space, which significantly reduces flow rate in the Disse space by up to 90.0%. RBC deformation in the sinusoid cavity was further investigated to illustrate how the specified microflow features are associated with typical cell deformation inside the sinusoids. When endothelial permeability was varied, both deformation index and initial deformation rate were altered significantly, leading to variations in deformation index of 26.7%. These systematic analyses of flow velocity, flow rate, and RBC deformation highlight the potential contributions of these regulating factors from numerical calculations.

In our study, a major finding is the biphasic pattern of shear stress on the surface of hepatocytes and on the lower side of endothelial cells in the Disse space (Fig. 4). The shear stress acting on hepatocytes was mainly affected by endothelial permeability coefficient and HMVCL thickness, yielding a biphasic regulation pattern. When the endothelial permeability is sufficiently high, increase in the thickness of the porous HMVCL on the surface of hepatocytes enhances the shear stress acting on hepatocytes, implying that the presence of hepatocyte microvilli augments the transmission of shear stress from the sinusoid cavity. By contrast, shear stress decreases with increases in HMVCL thickness when the endothelial permeability is low. Thus, the role of this porous layer in the microflow is similar to that of the glycocalyx in capillary flows. In general, the wall of capillary vessels is embedded with a layer of macromolecules, called the glycocalyx, which could cause endothelial dysfunction and cardiovascular disease when the layer is relatively thin (26,27). Numerical simulations of the effect of glycocalyx layer on capillary flow indicated that a thicker glycocalyx layer is associated with higher shear stress on the wall surface, which is beneficial to the functional implementation of endothelial cells (23,28). Under physiological conditions, hepatocyte microvilli perform functions similar to those of the glycocalyx layer, and the presence of the microvilli is conducive to

TABLE 3 Estimated offset of the maximal velocity along the channel height

	The offset of the lower channel
$\mu_{Rwall/}\mu = 0.0$	0.0%
$\mu_{Rwall/}\mu = 2.0$, H = 20 μm	6.0%
$\mu_{Rwall/}\mu = 2.0$, H = 30 μm	8.0%
$\mu_{Rwall/}\mu = 2.0$, H = 40 μm	10.0%
$\mu_{Rwall/}\mu = 2.0$, H = 50 μm	12.0%
$\mu_{Rwall/}\mu = 1.0$, H = 50 μm	8.0%
$\mu_{Rwall/}\mu = 1.5$, H = 50 μm	10.0%
$\mu_{Rwall/}\mu = 2.0$, H = 50 μm	12.0%
$\mu_{Rwall/}\mu = 2.5$, H = 50 μm	14.0%

lumen blood flow to hepatocytes and favorable to the transmission of mechanical signals. When liver lesions occur, endothelial capillarization occurs, permeability coefficient decreases, and a large amount of collagen is deposited in the Disse space (29,30). At this point, the shear stress on the surface of hepatocytes is quite low, and the thicker the collagen layer, the lower the shear stress. These observations indicated that the collagen layer impedes mechanical signal transmission of blood flow to hepatocytes. In addition, it can be seen from Eq. 18 that when the size of the Disse space is close to that of the sinusoid cavity, the flow velocity (also shear stress) in the Disse space increases with increase in collagen layer thickness, and the biphasic pattern of shear stress no longer exists. Thus, the size of the Disse space is a key factor in regulating shear stress in the Disse space, and this biphasic regulation pattern only appears in microflow in the Disse space. It must be noted that this model only incorporates a simplified hepatic sinusoid structure with uniform endothelial thickness and permeability coefficient. In fact, in vivo sinusoidal structures are more complicated not only by heterogeneous thickness and permeability, but also by time-dependent variations with related pathophysiological progress, which calls for future investigation. Meanwhile, compared with the in vivo 3D hepatic sinusoids, the irregular shape of the endothelium and the nonuniform sinusoidal diameter in actual physiology cannot be well realized in this simplified 2D modeling, which will be further considered by improving this 2D model and developing a 3D model with a curved sinusoidal lumen.

For application, the shift in flow velocity caused by wall roughness in the lower channel was further tested in a typical, dual-channel liver sinusoidal chip (29,30). Overall, our numerical calculations in the flow fields were consistent with previous experimental data. Furthermore, the velocity in the lower channel was found to be low and further decreased near the wall. The maximal velocity was offset by the presence of wall roughness. Increasing surface roughness enhanced flow resistance near the wall and caused the velocity profile to deviate from the wall, producing a maximal velocity deviation of 14%. In addition, fitting the experimental data with an empirical unitary cubic equation revealed a shift in the velocity profile. This deviated velocity distribution may alter the flow shear effect on cultured cells and further affect nutrient transport in the lower channel, thereby affecting cell growth and function. Therefore, our numerical analyses provide a basis for optimizing the future design of liver chips or organoids and corresponding experimental validation considering low flow velocity and potential experimental errors in the lower channel.

CONCLUSIONS

The characteristics of blood flow in hepatic sinusoids are closely associated with the physiological functions of hepatic cells and the occurrence of liver fibrosis. The contribution of microflow that originates from the micron-sized Disse space to flow in the sinusoids is particularly important, considering the roughness caused by hepatocyte microvilli and permeability mediated by the inherent endothelium and deposited collagen. These microflow features in the sinusoids are critical to correlate the profiles of flow velocity (rate) and shear stress with endothelial permeability and HMVCL roughness. The impacts of several parameters—permeability coefficient and thickness of endothelial layers and HMVCLs—on the flow field were analyzed numerically to identify the dominant factors of endothelial permeability in flow-velocity profiling and HMVCL thickness in the biphasic shear stress pattern. These calculations not only provide a reference for elaborating on microflow features in sinusoids but also are applicable in understanding the roles of blood flow under cell deformation inside sinusoids and for the design of in vitro liver chips.

SUPPORTING MATERIAL

Supporting material can be found online at https://doi.org/10.1016/j.bpj.2021.09.020.

AUTHOR CONTRIBUTIONS

S.L. and M.L. designed the study. T.W. and Y.C. developed analytical theory and completed the simulation. Y.H. and Z.S. analyzed the data. T.W. and Y.C. wrote the manuscript. S.L. and M.L. edited the manuscript and approved the final draft.

ACKNOWLEDGMENTS

The authors are grateful for Drs. Shenbao Chen, Lüwen Zhou, and Shiliang Feng for technical assistance and helpful discussions.

This work was supported by National Natural Science Foundation of China (grant no. 11972252), Frontier Science Key Project of Chinese Science Academy (grant QYZDJ-SSW-JSC018), and Tianjin Natural Science Foundation (grant no. 17JCYBJC29300).

REFERENCES

1. Ricken, T., D. Werner, …, O. Dirsch. 2015. Modeling function-perfusion behavior in liver lobules including tissue, blood, glucose, lactate and glycogen by use of a coupled two-scale PDE-ODE approach. *Biomech. Model. Mechanobiol.* 14:515–536.
2. DeLeve, L. D. 2015. Liver sinusoidal endothelial cells in hepatic fibrosis. *Hepatology.* 61:1740–1746.
3. Li, Y., L. Yong, …, Y. Lu. 2014. The correlation between the TCM syndromes of cirrhosis and the degree of collagenous fiber deposition in the peri-sinus space. *World Journal of Integrated Traditional and Western Medicine.* 9:607–610.
4. Yan, W., Y. Liu, and B. Fu. 2019. LBM simulations on the influence of endothelial SGL structure on cell adhesion in the micro-vessels. *Comput. Math. Appl.* 78:1182–1193.
5. Li, P., J. Zhou, …, M. Long. 2020. Characterizing liver sinusoidal endothelial cell fenestrae on soft substrates upon AFM imaging and deep learning. *Biochim. Biophys. Acta Gen. Subj.* 1864:129702.

6. Shetty, S., C. J. Weston, …, P. F. Lalor. 2014. A flow adhesion assay to study leucocyte recruitment to human hepatic sinusoidal endothelium under conditions of shear stress. *J. Vis. Exp* 51330.
7. Greuter, T., and V. H. Shah. 2016. Hepatic sinusoids in liver injury, inflammation, and fibrosis: new pathophysiological insights. *J. Gastroenterol.* 51:511–519.
8. Koo, J., and C. Kleinstreuer. 2003. Liquid flow in microchannels: experimental observations and computational analyses of microfluidics effects. *J. Micromech. Microeng.* 13:568–579.
9. Hetsroni, G., A. Mosyak, …, L. P. Yarin. 2005. Fluid flow in micro-channels. *Int. J. Heat Mass Transf.* 48:1982–1998.
10. Vanheule, E., A. M. Geerts, …, I. Colle. 2008. An intravital microscopic study of the hepatic microcirculation in cirrhotic mice models: relationship between fibrosis and angiogenesis. *Int. J. Exp. Pathol.* 89:419–432.
11. Fan, J., C.-J. Chen, …, W.-G. Zhang. 2019. Hemodynamic changes in hepatic sinusoids of hepatic steatosis mice. *World J. Gastroenterol.* 25:1355–1365.
12. Illa, X., S. Vila, …, R. Villa. 2014. A novel modular bioreactor to in vitro study the hepatic sinusoid. *PLoS One.* 9:e111864.
13. Liu, Y., J. Wei, …, X. Li. 2016. Micropatterned coculture of hepatocytes on electrospun fibers as a potential in vitro model for predictive drug metabolism. *Mater. Sci. Eng. C.* 63:475–484.
14. Du, Y., N. Li, …, M. Long. 2017. Mimicking liver sinusoidal structures and functions using a 3D-configured microfluidic chip. *Lab Chip.* 17:782–794.
15. Rani, H. P., T. W. H. Sheu, …, P. C. Liang. 2006. Numerical investigation of non-Newtonian microcirculatory blood flow in hepatic lobule. *J. Biomech.* 39:551–563.
16. Sharifi, F., B. Firoozabadi, …, K. Firoozbakhsh. 2015. Numerical modeling of ureagenesis in a microfluidic channel mimicking a liver lobule. *In* 2015 22nd Iranian Conference on Biomedical Engineering (ICBME). IEEE, pp. 54–59.
17. Shi, Z., S. K. Chapes, …, C. H. Wu. 2016. An agent-based model of a hepatic inflammatory response to Salmonella: a computational study under a large set of experimental data. *PLoS One.* 11:e0161131.
18. Guo, Z., and T. S. Zhao. 2002. Lattice Boltzmann model for incompressible flows through porous media. *Phys. Rev. E Stat. Nonlin. Soft Matter Phys.* 66:036304.
19. Kleinstreuer, C., and J. Koo. 2004. Computational analysis of wall roughness effects for liquid flow in micro-conduits. *J. Fluids Eng.* 126:1–9.
20. Tsubota, K., S. Wada, and T. Yamaguchi. 2006. Particle method for computer simulation of red blood cell motion in blood flow. *Comput. Methods Programs Biomed.* 83:139–146.
21. Verhaeghe, F., L. Luo, and B. Blanpain. 2009. Lattice Boltzmann modeling of microchannel flow in slip flow regime. *J. Comput. Phys.* 228:147–157.
22. Tong, C. Q., Y. L. He, …, Y. W. Liu. 2007. Mass modified outlet boundary for a fully developed flow in the lattice Boltzmann equation. *Int. J. Mod. Phys. C.* 18:1209–1221.
23. Secomb, T. W., R. Hsu, and A. R. Pries. 2002. Blood flow and red blood cell deformation in nonuniform capillaries: effects of the endothelial surface layer. *Microcirculation.* 9:189–196.
24. Hosseini, S. M., and J. J. Feng. 2009. A particle-based model for the transport of erythrocytes in capillaries. *Chem. Eng. Sci.* 64:4488–4497.
25. Mohiuddin Mala, G., and D. Li. 1999. Flow characteristics of water in microtubes. *Int. J. Heat Fluid Flow.* 20:142–148.
26. Gouverneur, M., B. Berg, …, H. Vink. 2006. Vasculoprotective properties of the endothelial glycocalyx: effects of fluid shear stress. *J. Intern. Med.* 259:393–400.
27. Nieuwdorp, M., T. W. van Haeften, …, E. S. Stroes. 2006. Loss of endothelial glycocalyx during acute hyperglycemia coincides with endothelial dysfunction and coagulation activation in vivo. *Diabetes.* 55:480–486.
28. Zhang, S., X. Zhang, …, H. Lipowsky. 2015. Influence of thickness and permeability of endothelial surface layer on transmission of shear stress in capillaries. *Sci. China Phys. Mech. Astron.* 58:1–9.
29. Shetty, S., P. F. Lalor, and D. H. Adams. 2018. Liver sinusoidal endothelial cells - gatekeepers of hepatic immunity. *Nat. Rev. Gastroenterol. Hepatol.* 15:555–567.
30. van der Graaff, D., W. J. Kwanten, and S. M. Francque. 2019. The potential role of vascular alterations and subsequent impaired liver blood flow and hepatic hypoxia in the pathophysiology of non-alcoholic steatohepatitis. *Med. Hypotheses.* 122:188–197.